Application of time-variable process noise in terrestrial reference frames determined from VLBI data

Benedikt Soja[a,*], Richard S. Gross[a], Claudio Abbondanza[a], Toshio M. Chin[a], Michael B. Heflin[a], Jay W. Parker[a], Xiaoping Wu[a], Kyriakos Balidakis[b], Tobias Nilsson[b], Susanne Glaser[b], Maria Karbon[c], Robert Heinkelmann[b], Harald Schuh[b,d]

[a] *Jet Propulsion Laboratory, California Institute of Technology, Pasadena, United States of America*
[b] *GFZ German Research Centre for Geosciences, Potsdam, Germany*
[c] *University of Bonn, Institute of Geodesy and Geoinformation, Bonn, Germany*
[d] *Technische Universität Berlin, Institute for Geodesy and Geoinformation Science, Berlin, Germany*

Abstract

In recent years, Kalman filtering has emerged as a suitable technique to determine terrestrial reference frames (TRFs), a prime example being JTRF2014. The time series approach allows variations of station coordinates that are neither reduced by observational corrections nor considered in the functional model to be taken into account. These variations are primarily due to non-tidal geophysical loading effects that are not reduced according to the current IERS Conventions (2010). It is standard practice that the process noise models applied in Kalman filter TRF solutions are derived from time series of loading displacements and account for station dependent differences. So far, it has been assumed that the parameters of these process noise models are constant over time. However, due to the presence of seasonal and irregular variations, this assumption does not truly reflect reality. In this study, we derive a station coordinate process noise model allowing for such temporal variations. This process noise model and one that is a parameterized version of the former are applied in the computation of TRF solutions based on very long baseline interferometry data. In comparison with a solution based

*Corresponding author
Email address: bsoja@jpl.nasa.gov (Benedikt Soja)

on a constant process noise model, we find that the station coordinates are affected at the millimeter level.

Keywords: Terrestrial reference frames, VLBI, Kalman filter, non-tidal loading, process noise

1. Introduction

Kalman filtering has become an established approach for the determination of terrestrial reference frames (TRFs). Recently, JTRF2014 (Abbondanza et al., 2017) by the International Earth Rotation and Reference Systems Service (IERS) International Terrestrial Reference System (ITRS) Combination Center at Jet Propulsion Laboratory (JPL) has been released as a candidate solution for the International Terrestrial Reference Frame (ITRF). JTRF2014 was computed using the software KALREF (Wu et al., 2015), based on Kalman filter and smoother algorithms. The time series nature of the solution allows irregular and short-term variations in the station coordinates of the space-geodetic techniques to be taken into account and has been shown to reliably represent non-tidal station loading and geocenter motion (Zelensky et al., 2018). Coordinate predictions can be calculated by extrapolating the functional model, which includes linear and seasonal terms in the case of the JTRF2014.

In Kalman filter TRF solutions like the JTRF2014, certain amounts of process noise are applied, controlling the magnitude of the temporal coordinate variations of the individual stations. The process noise model, which comprises the process noise values for the different parameters estimated in the filter, is conventionally derived from three-dimensional time series of geophysical non-tidal loading displacements, with station-dependent differences taken into account. Soja et al. (2016) additionally scaled the process noise values for certain stations during times of severe post-seismic deformations. Aside from earthquake-related modifications, process noise has so far always been assumed constant over time when determining TRFs.

However, the stochastic properties of geophysical loading displacements exhibit temporal variations over various time scales, which ideally should be accounted for when using these data to create a model of process noise. An improvement in the noise model should yield an increase in the accuracy of the TRF's station coordinates, which is, for example, of great interest in navigation tasks or geophysical investigations (Plag and Pearlman, 2009).

Since no ground truth data is available, assessing the accuracy of station coordinates is a delicate issue (Collilieux et al., 2014). At the very least, it is worth to assess the impact of assuming constant or time-variable process noise on the resulting TRF station coordinates to give recommendations for future TRF realizations. For this reason, we derive (Section 2) and apply (Section 3) for the first time a process noise model for station coordinates that is time-dependent for every single station. We conduct our investigations based on very long baseline interferometry (VLBI) data, but the results should be in large parts transferable to other space geodetic techniques and combinations thereof.

2. Time-dependent process noise model

The process noise model utilized in Kalman filter reference frames is conventionally based on the assumption that irregular variations in the coordinates are caused by unmodeled non-tidal loading displacements. According to the IERS Conventions (2010), the non-tidal displacements due to the atmosphere (NTAL), oceans (NTOL), and hydrology (HYDL) should not be corrected in the analysis of space-geodetic techniques and are therefore the constituents of station coordinate process noise models.

2.1. Geophysical loading data

In this study, time series of NTAL, NTOL, and HYDL between 1985 and the end of 2015 as provided by Helmholtz Centre Potsdam – GFZ German Research Centre for Geosciences (Dill and Dobslaw, 2013)[1] are used to derive the process noise models. For every VLBI site (cf. Section 3.1), the sum of the three displacement time series is computed with a temporal resolution of 1 day. Additionally, trend and annual signal are removed, since they are commonly parameterized and estimated as part of the functional model unlike the random coordinate variations the process noise model aims to address. As an example, Fig. 1 shows the sum of the loading displacements for station Algonquin Park, Canada after trend and annual signals have been removed. Here, the temporal variability of the residual displacements is one of the largest among the VLBI stations. Harmonic signals at other periods than annual, such as semi-annual or to a lesser extent five-yearly, are discernible as well in the case of Algonquin Park, but removing them would not

[1] http://www.gfz-potsdam.de/en/esmdata/loading/

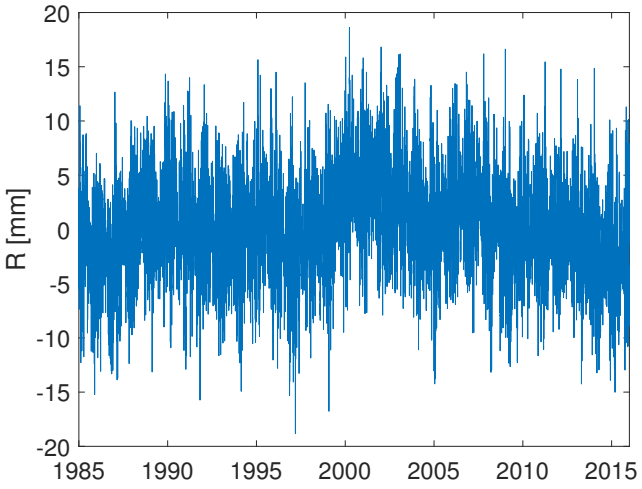

Figure 1: Sum of the time series of non-tidal loading deformations at station Algonquin Park, radial component, with trend and annual signal removed

significantly affect the noise estimates, which are derived from time differences of only a few days (c.f. next section). Even removing annual signals is not required when considering such short time differences, since the process noise would only be affected at the 1 part-per-million level (as found in test solutions). If the process noise was derived based on different assumptions, the handling of long-periodic signals would be more critical.

2.2. Derivation of process noise models

The derivation of process noise models followed the methodology established in Soja et al. (2016). Assuming random walk (RW) processes for station coordinate variations, the Allan standard deviation (ADEV, σ_y) was used to compute the power spectral densities (PSD, Φ) of white noise driving the random walks utilized in the Kalman filter: $\Phi_{\mathrm{RW}} = \sigma_y^2(\tau) \cdot \tau$ with time differences $\tau \in \{1, 2, 3, 4\}$ days. We selected this time range since it is the typical interval between VLBI experiments used within this study and thus the state updates in the Kalman filter, and because in this time range the ADEV most closely resembles a random walk process. Each PSD value is thus estimated based on four ADEV values.

In order to derive a temporally constant process noise model, the whole 31-year time span of loading data was used to compute the ADEV values, and consequently the PSD (for every single station). For the time-dependent

model, we decided to split the loading time series into monthly chunks. For every single month and station, the individual values for ADEV and PSD were derived. The monthly interval seemed to be a good balance between a reasonable temporal resolution of the resulting model on the one side and sufficient data points to reliably compute the ADEV on the other side.

The monthly ADEV curves for station Algonquin park, radial component, are shown in Fig. 2. The stochastic behavior is on average (c.f. dark blue curve) between a random walk (for $\tau \leq 4$ days) and a white noise process (for larger time differences). A fit of the average ADEV values for the considered time differences (red line) reveals a power-law exponent of -0.82 (white noise: -1, RW: -0.5).

The selection of the type of process noise for station coordinates (in this study: random walk) is a compromise since it is very difficult to efficiently model the exact stochastic properties of the non-tidal loading data. For example, using white noise to fit the longer time differences would result in inflated noise at shorter intervals, and would allow artificial errors at high frequencies to leak into the TRF coordinates. A detailed discussion on this issue is provided in Soja et al. (submitted).

The monthly PSD values for Algonquin Park are visualized in Fig. 3, red curve. Linear and annual signals based on the monthly PSD values were estimated for every single station. In addition to the constant and monthly process noise models, the fitted PSD (linear plus annual) is the third process noise model we investigate in this study. The parameters of the latter model, as estimated from the monthly PSD values, are provided in the supplementary material.

2.3. Analysis of process noise time series

In the following, the PSD time series (cf. Fig. 3) of the individual stations are analyzed. We present only the results for the radial coordinate components, since the signals are usually four to six times larger than for the horizontal ones. When applied in the Kalman filter, the three-dimensional process noise models are used.

Figure 4 shows the mean values of the monthly time series. The temporal variability of atmospheric pressure is higher at mid and high latitudes than in equatorial regions and consequently, the PSD is generally larger at higher latitudes and in continental areas, considering the fact that the displacement caused by non-tidal atmospheric pressure loading is larger than the other non-tidal loading effects. The difference in the average PSD between the

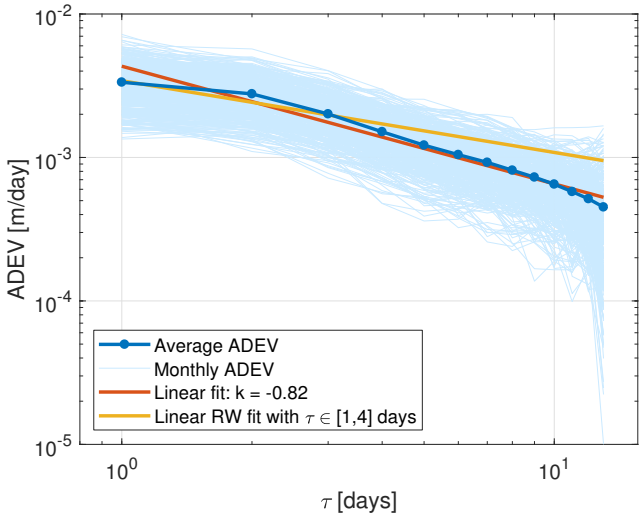

Figure 2: Based on the time series of radial loading displacements at Algonquin Park, the ADEV is shown for every single month between 1985 and 2015 (thin light blue lines), an average thereof (dark blue), a linear fit resulting in a slope of -0.82 (red), as well as a linear fit assuming a random walk ($k = -0.5$) for time differences of 1–4 days (yellow)

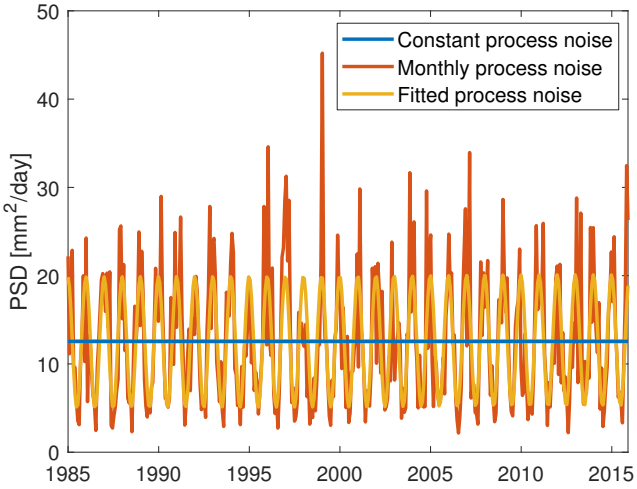

Figure 3: Constant PSD value derived from 31 years (blue), monthly PSD time series (red), and a linear and annual fit of the monthly values (yellow) for Algonquin Park, radial component

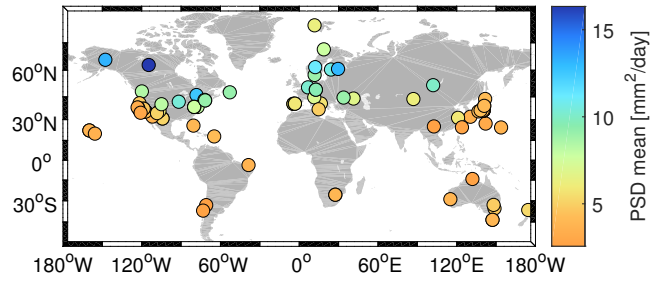

Figure 4: Map with color-coded mean values of the monthly PSD, radial component

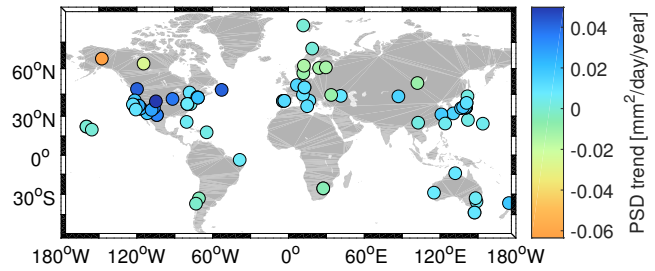

Figure 5: Map with color-coded trend derived from the PSD time series in radial direction

individual stations amounts to a factor of four. The standard deviation of the monthly PSD shows the same pattern as the mean and is therefore not visualized here. Evidently, locations with larger average noise are subject to larger temporal variations in the noise. While the mean PSD ranges from 2.5 to 16.3 mm^2/day, the standard deviation amounts to 0.9–9.1 mm^2/day. In the case of the horizontal components, the different stations have mean PSD values between 0.9–2.1 mm^2/day with standard deviations between 0.4–0.8 mm^2/day (not shown here).

The long-term trends in process noise as estimated from the time series are indicated in Fig. 5. On average, there is a slight increase over time of 0.01 mm^2/day/year. Over 31 years, this change amounts to a difference of 5% in the average noise. The largest change is found for station Gilmore Creek, Alaska with an average reduction of the PSD of 10% over 31 years. The maximum trends in both horizontal components are one order of magnitude smaller than for the radial component.

The estimated annual signals are much more pronounced than the trends, as for example visible in Fig. 3 for Algonquin Park. On average, they amount to 37% of the average PSD. The spatial patterns of the annual amplitude

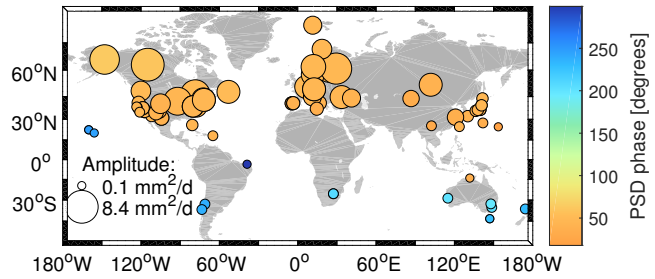

Figure 6: Map with amplitude (size) and phase (color) of the annual signals of the radial PSD values

(Fig. 6) are very similar to those for the mean and standard deviation. The small amplitudes in the southern hemisphere are related to the fact that most stations are close to the ocean, where the NTAL displacements are weaker because of the inverted barometer assumption applied for stations near the coast (Petrov and Boy, 2004). The phases are in line with the seasons on the two hemispheres, i.e. a shift of 180° between the northern and southern hemisphere. Deviations in the phase are seen only for locations with small amplitudes, for which the phases are not as reliable. While the radial component exhibits annual amplitudes in PSD of up to 8 mm^2/day, the horizontal ones remain below 0.3 mm^2/day.

3. Effect on TRF solutions

The analysis of the monthly process noise time series revealed that there are significant temporal variations. In the following, the effect of time-dependent process noise models on the resulting VLBI TRFs (VTRFs) is studied.

3.1. VLBI TRF solutions

The software for computing the VTRFs is based on a Kalman filter and smoother, as described in Soja et al. (2016). The coordinate model was chosen to be linear (coordinate offset + velocity), since Soja et al. (submitted) did not find significant improvements when additionally estimating seasonal signals in VTRFs in the case of constant process noise. The coordinate offsets were assumed to behave like random walk processes and the velocities were treated deterministically. The state of the Kalman filter was updated for every single VLBI session, i.e. usually every 1–4 days.

We selected VLBI data from 3992 VLBI sessions between 1985 and the end of 2015 (covering the same time span as the loading data) and from 84 globally distributed stations to compute our VTRF solutions. The locations of the stations are visible in Figs. 4–6, the majority of them in the northern hemisphere. The VLBI data was provided by the International VLBI Service for Geodesy and Astrometry (IVS, Nothnagel et al., 2016). First, the VLBI sessions were analyzed with the least-squares module of VieVS@GFZ (Nilsson et al., 2015) and station coordinates were estimated per session, together with parameters for the troposphere, station clocks, Earth's orientation, and radio source positions. The session-wise station coordinates, along with their covariance matrices, served as input to the Kalman filter and smoother.

Three VTRF solutions were computed, differing only by the process noise model that was applied within the filter:

- Constant process noise (S1, cf. blue curve in Fig. 3)
- Monthly process noise (S2, cf. red curve in Fig. 3)
- Fitted process noise (S3, cf. yellow curve in Fig. 3)

3.2. Comparison of VTRFs

As an example, the three VTRF coordinate time series for station Algonquin Park during the time span of uninterrupted observations are depicted in Fig. 7. The different process noise models result in coordinate differences too small to study in detail, which are therefore, w.r.t. S1, separately plotted in Fig. 8. The differences reach several mm (up to 1 cm) at epochs when the original coordinate time series has larger peaks

The VLBI station in Kokee Park, Hawaii (Figs. 9 and 10) was selected as a second example. Located on an island (inverse barometer effect) and much closer to the equator, it is very differently affected by loading deformations than the one in Algonquin Park. The average PSD of Kokee Park for the radial component is about 3.5 times smaller than the one of Algonquin Park. The absolute differences reach about 5 mm, a bit less than for Algonquin Park. As expected, the VTRF solution with the linear and annual process noise model is closer to the one with the constant model, since the PSD does not deviate as much from a constant value compared to the monthly PSD time series.

A histogram of all the radial coordinate differences between the solutions with time-dependent process noise and the one with constant process noise

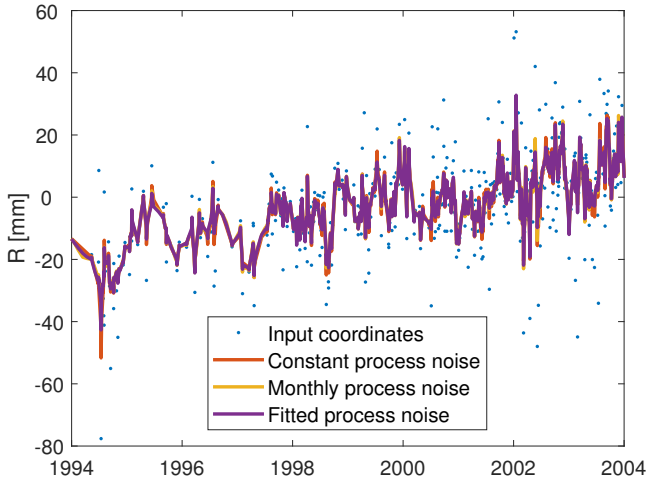

Figure 7: Station coordinate time series of Algonquin Park, radial component: single-session VLBI coordinates (blue dots) as well as Kalman filter VTRF solutions S1 (red), S2 (yellow), and S3 (purple)

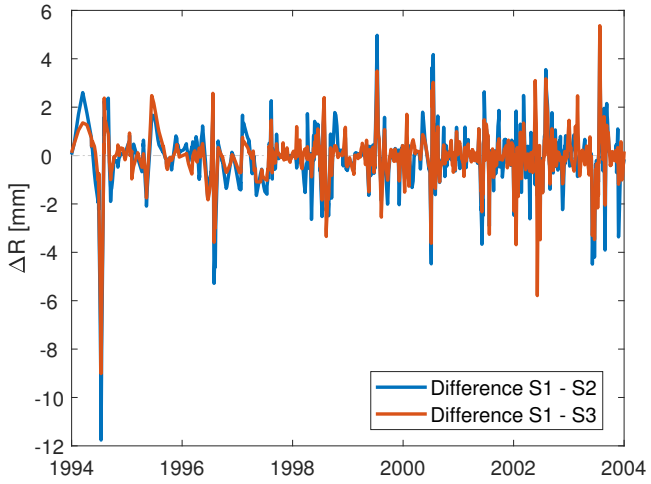

Figure 8: Radial coordinate differences between the solutions portrayed in Fig. 7 (Algonquin Park)

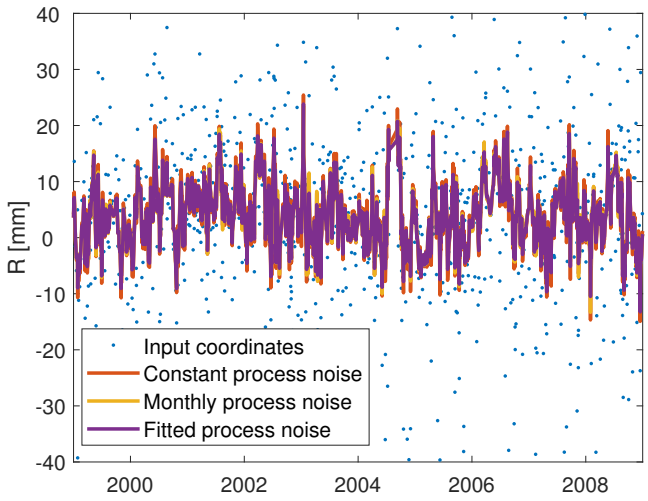

Figure 9: The same features as in Fig. 7, but for Kokee Park

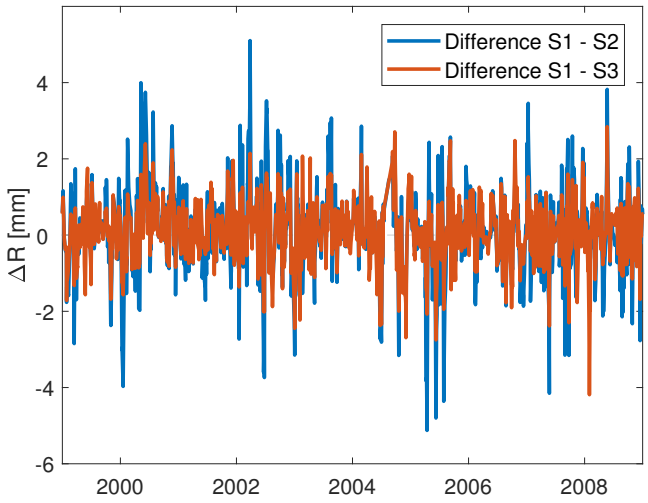

Figure 10: Radial coordinate differences between the solutions depicted in Fig. 9 (Kokee Park)

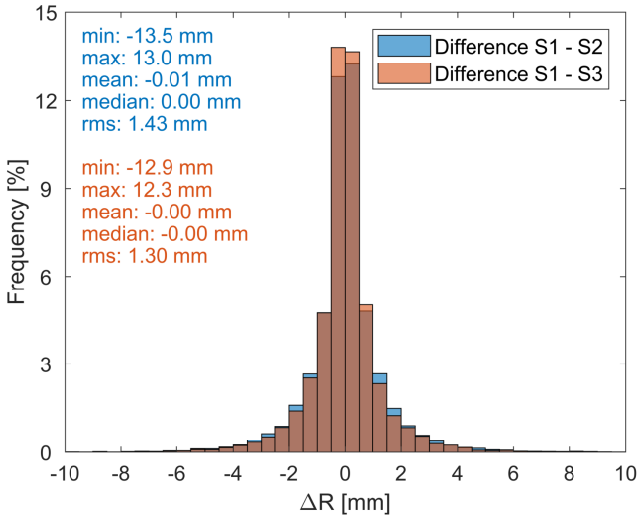

Figure 11: Histogram of the radial coordinate differences from all stations (16542 coordinate differences in total)

is provided in Fig. 11. The differences are centered around zero, with mean and median of less than 0.01 mm, which means that no significant biases are introduced when different process noise models are used. Still, the difference are not negligible with 28% larger than 1 mm. The RMS of the differences is a bit above 1 mm for both solutions with time-dependent process noise.

To assess the average effect of the process noise models on TRF defining parameters, the scale and coordinate residuals of a seven-parameter Helmert transformation between the VTRF solutions and the single-session VLBI coordinates were analyzed. Fig. 12 shows the individual scale estimates together with moving averages. While small differences are visible in the session-wise scale estimates, the moving averages of the different VTRF solutions' scales appear to be almost identical. Fig. 13 shows the differences of the scale estimates between the different solutions, highlighting that the scale differences are at the millimeter level for individual sessions. Statistics on the scale estimates are given in Table 1, highlighting that the weighted mean (weighted by the inverse of the squared formal errors) of the scale estimates differs by only 0.01 mm. In terms of the weighted RMS (WRMS), the differences are close to 0.1 mm.

WRMS values of residuals from the Helmert transformation are provided in Table 2 for every coordinate component. The impact of the different pro-

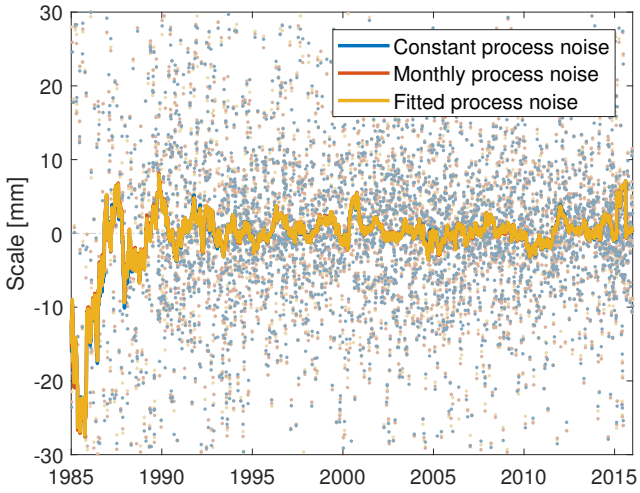

Figure 12: Scale estimates from a Helmert transformation between single-session VLBI coordinates and three VTRF solutions (S1, S2, and S3). Individual estimates are shown as shaded dots, while 180-day moving averages are depicted as curves. The blue and red curves are hidden behind the yellow one

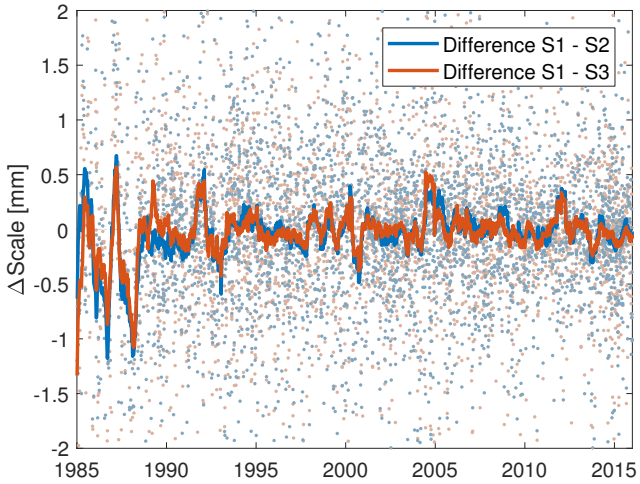

Figure 13: Differences between scale estimates of solutions based on time-variable process noise w.r.t. the one based on constant process noise. The undifferenced values are shown in Fig. 12. Single-session differences are shown as shaded dots, while 180-day moving averages of the differences are depicted as curves

Table 1: Weighted mean and WRMS of scale estimates, based on seven-parameter Helmert transformations using all stations (cf. Fig. 12), in units of mm

Solution	WMEAN	WRMS
S1	0.11	5.41
S2	0.10	5.34
S3	0.12	5.33
Difference S1 − S2	0.01	0.07
Difference S1 − S3	−0.01	0.08

Table 2: WRMS values of the residuals of a Helmert transformation between single-session VLBI coordinates and VTRF solutions in mm

Solution	Radial	East	North	3-D
S1	3.38	1.66	1.95	4.57
S2	3.34	1.63	1.94	4.50
S3	3.36	1.65	1.97	4.55
Difference S1 − S2	0.04	0.03	0.01	0.07
Difference S1 − S3	0.02	0.01	−0.02	0.02

cess noise models tends to be largest for the radial component, which is most affected by the loading deformations. The three-dimensional WRMS values differ by similar amounts compared to the scale WRMS (0.02–0.07 mm).

It should be noted that smaller WRMS values in this context do not necessarily mean that the solution is better, it just shows that the TRF coordinates are on average closer to the single-session coordinates. Simply choosing larger average process noise values has the same effect. If process noise values were used that are larger than what the geophysical signals indicate, the differences between the coordinates from the TRF and the individual VLBI sessions might decrease, however, it is likely that artificial noise from observational errors or network turnaround is absorbed in the TRF station coordinates.

The main reason that the impact of time-dependent process noise as presented in Tables 1 and 2 appears to be negligible is that the noise variations are mostly cyclic and are averaged out when considering the whole time span. Therefore, we additionally computed the 3-D WRMS values of the transfor-

Table 3: Monthly three-dimensional WRMS [mm] of transformation residuals. Additionally, the radial PSD [mm^2/day], averaged over the whole time span, is given on a monthly basis (average over all months: 5.92 mm^2/day)

Month	PSD	3-D WRMS [mm]				
	[mm^2/day]	S1	S2	S3	S1 − S2	S1 − S3
January	7.82	5.27	5.02	4.90	0.25	0.37
February	7.62	4.10	3.92	3.93	0.18	0.17
March	7.78	4.03	3.86	3.86	0.17	0.17
April	7.01	5.34	5.32	5.39	0.02	-0.05
May	5.67	4.74	4.88	4.79	-0.14	-0.05
June	4.25	6.82	7.74	7.66	-0.92	-0.84
July	3.63	5.60	6.14	6.07	-0.54	-0.47
August	3.68	5.55	6.05	5.97	-0.50	-0.42
September	4.20	5.46	5.70	5.69	-0.24	-0.23
October	5.12	7.15	7.40	7.38	-0.25	-0.23
November	6.47	4.94	4.85	4.87	0.09	0.07
December	7.71	5.43	5.20	5.13	0.23	0.30

mation residuals for individual months, while still averaging over the 31 years for reliability (Table 3, with the differences visualized in Fig. 14). The largest difference between the solutions with constant and time-dependent noise is in June, with almost 1 mm, and July and August with about 0.5 mm. Additionally shown are the radial PSD values averaged over all stations and it becomes evident that the increased WRMS difference in northern hemisphere summer is directly related to smaller than average PSD values. Similarly, the WRMS differences are larger in winter, up to 0.4 mm. The annual cycle is shifted between the northern and southern hemispheres by six months, which attenuates the maximal differences seen in Table 3. The effect would be even more pronounced when only stations from the same hemisphere were considered. The correlation between the monthly averaged PSD and the differences in WRMS w.r.t. S1 are 90% (S2) and 89% (S3), both with p-values of 10^{-4}. The correlation even increases to 97% / 95% when June is excluded. The correlation for the solution based on the monthly process noise model is thus slightly higher, but the one with the fitted model is very close. The difference in WRMS between the VTRFs based on the monthly PSD model and the fitted one is less than 0.1 mm for all months.

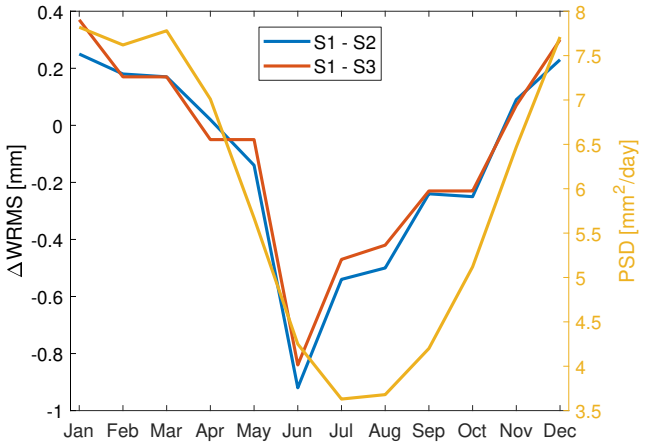

Figure 14: Three-dimensional WRMS differences of solutions S2 and S3 w.r.t. S1 for individual months as provided in Table 3 (left Y-axis), overlaid with monthly PSD values (right Y-axis)

4. Conclusion

In this study, we have for the first time utilized time-dependent process noise models based on loading displacements in the determination of Kalman filter TRF solutions. The models feature larger average noise values, noise variability, and annual amplitudes in higher latitudes and continental areas since the noise is primarily affected by non-tidal atmospheric pressure loading. On average, the process noise slightly increases over time, but the seasonal signal component is about one order of magnitude larger than the trend.

Averaged over 31 years, the cyclic effect of time-dependent process noise on the TRF coordinates cancels out and results in WRMS differences at the level of only 0.01 mm. The long-term behavior of station coordinates of Kalman filter TRF solutions with constant or time-dependent process noise models is therefore largely consistent.

One of the main advantages of a Kalman filter TRF is the ability to take into account short-term coordinate variations. Here, TRF coordinates of individual VLBI stations differ by up to 1 cm between solutions with monthly and constant process noise models. Almost a third of radial station coordinate differences is above 1 mm. Considering individual months, the difference in 3-D WRMS of Helmert transformation residuals almost reaches 1 mm when averaged over all stations. The effect of applying a time-dependent process

noise model is thus not negligible. Since such a model is more consistent with the expected geophysical signals manifested in station coordinates compared to a constant one, we recommend its implementation in future Kalman filter TRF solutions.

Finally, we found that a parameterized process noise model (linear plus annual, c.f. supplementary material) leads to very similar results compared to a monthly time series of process noise values, with the advantage that it can easily be extrapolated into the future or the past.

While our results were obtained from VLBI data only, time-dependent process noise should be similarly important for TRF solutions based on data from other space-geodetic techniques and combinations thereof. Nevertheless, it would be important to investigate whether technique-specific systematic errors would be differently absorbed in the estimated parameters due to (mostly) seasonally varying process noise and if so, to what extent. A dedicated study on the application of time-dependent process noise in the framework of a four-technique JTRF-like solution could shed light on this issue.

Acknowledgements

The authors thank the IVS for providing the VLBI data (Nothnagel et al., 2015) and GFZ Potsdam for making available the loading data (Dill and Dobslaw, 2013) used in this work. B. Soja's research was supported by an appointment to the NASA Postdoctoral Program, administered by Universities Space Research Association, at the Jet Propulsion Laboratory, California Institute of Technology, under a contract with the National Aeronautics and Space Administration. We thank the editor Dr. Pascal Willis and two anonymous reviewers for their helpful comments on the manuscript.

Abbondanza, C., Chin, T.M., Gross, R.S., Heflin, M.B., Parker, J.W., Soja, B.S., van Dam, T., Wu, X., 2017. JTRF2014, the JPL Kalman Filter and Smoother Realization of the International Terrestrial Reference System. Journal of Geophysical Research: Solid Earth 122, 8474–8510. doi:10.1002/2017JB014360.

Collilieux, X., Altamimi, Z., Argus, D., Boucher, C., Dermanis, A., Haines, B., Herring, T., Kreemer, C., Lemoine, F., Ma, C., et al., 2014. External evaluation of the Terrestrial Reference Frame: report of the task force

of the IAG sub-commission 1.2, in: Earth on the Edge: Science for a Sustainable Planet. Springer, pp. 197–202.

Dill, R., Dobslaw, H., 2013. Numerical simulations of global-scale high-resolution hydrological crustal deformations. Journal of Geophysical Research: Solid Earth 118, 5008–5017. doi:10.1002/jgrb.50353.

IERS Conventions, 2010. G. Petit and B. Luzum (eds.). IERS Technical Note 36. Frankfurt am Main: Verlag des Bundesamtes für Kartographie und Geodäsie.

Nilsson, T., Soja, B., Karbon, M., Heinkelmann, R., Schuh, H., 2015. Application of Kalman filtering in VLBI data analysis. Earth, Planets and Space 67, 136. doi:10.1186/s40623-015-0307-y.

Nothnagel, A., Artz, T., Behrend, D., Malkin, Z., 2016. International VLBI service for geodesy and astrometry. Journal of Geodesy 91, 711–721. doi:10.1007/s00190-016-0950-5.

Nothnagel, A., et al., 2015. The IVS data input to ITRF2014. International VLBI Service for Geodesy and Astrometry, GFZ Data Services. doi:10.5880/GFZ.1.1.2015.002.

Petrov, L., Boy, J.P., 2004. Study of the atmospheric pressure loading signal in very long baseline interferometry observations. Journal of Geophysical Research: Solid Earth 109, B03405. doi:10.1029/2003JB002500.

Plag, H.P., Pearlman, M. (Eds.), 2009. Global Geodetic Observing System: Meeting the Requirements of a Global Society on a Changing Planet in 2020. Springer, Berlin, Heidelberg.

Soja, B., Gross, R.S., Abbondanza, C., Chin, T.M., Heflin, M.B., Parker, J.W., Wu, X., Nilsson, T., Glaser, S., Balidakis, K., Heinkelmann, R., Schuh, H., submitted. On the long-term stability of TRF solutions based on Kalman filtering. Journal of Geodesy .

Soja, B., Nilsson, T., Balidakis, K., Glaser, S., Heinkelmann, R., Schuh, H., 2016. Determination of a terrestrial reference frame via Kalman filtering of very long baseline interferometry data. Journal of Geodesy 90, 1311–1327. doi:10.1007/s00190-016-0924-7.

Wu, X., Abbondanza, C., Altamimi, Z., Chin, T.M., Collilieux, X., Gross, R.S., Heflin, M.B., Jiang, Y., Parker, J.W., 2015. KALREFA Kalman filter and time series approach to the International Terrestrial Reference Frame realization. Journal of Geophysical Research: Solid Earth 120, 3775–3802. doi:10.1002/2014JB011622.

Zelensky, N.P., Lemoine, F.G., Beckley, B.D., Chinn, D.S., Pavlis, D., 2018. Impact of ITRS 2014 Realizations on Altimeter Satellite Precise Orbit Determination. Advances in Space Research 61, 45–73. doi:10.1016/j.asr.2017.07.044.

Copyright 2017. All rights reserved.